

Observation number correlation in WMAP data

Ti-Pei Li^{1,2*}, Hao Liu^{1,†}, Li-Ming Song¹, Shao-Lin Xiong^{1,3} and Jian-Yin Nie¹

¹Key Laboratory of Particle Astrophysics, Institute of High Energy Physics, Chinese Academy of Sciences, Beijing, China

²Center for Astrophysics, Tsinghua University, Beijing, China

³Graduate School of Chinese Academy of Sciences, Beijing, China

ABSTRACT

A remarkable similarity between the large-scale non-Gaussian pattern of cosmic microwave background (CMB) temperatures obtained by Wilkinson Microwave Anisotropy Probe (WMAP) mission and the distribution feature of observation numbers is noted. Motivated from such a similarity, in this work we check the WMAP data for the correlation between pixel temperature t and observation number N . Systematic effect of imbalance differential observation and significant t - N correlation in magnitude, distribution non-Gaussianity and north-south asymmetry are found. Our results indicate that, for precision cosmology study based on WMAP observations, the observation effect on released WMAP temperature maps has to be further carefully studied.

Key words: cosmic microwave background — cosmology: observations — methods: data analysis

1 INTRODUCTION

The WMAP observations provide precision data for cosmology study. By analyzing CMB maps from the first year WMAP (WMAP1) data, Tegmark et al. (2003) find both the CMB quadrupole and octopole having power along a particular spatial axis and more works (de Oliveira-Costa et al. 2004; Eriksen et al. 2004a; Schwarz et al. 2004; Jaffe et al. 2005) find that the axis of maximum asymmetry tends to lie close to the ecliptic axis. A similar anomaly was also found in COBE maps (Copi et al. 2006). The unexplained orientation of large-scale patterns of CMB maps in respect to the ecliptic frame is one of the biggest surprises in CMB studies (Starkman and Schwarz 2005). A notable asymmetry of temperature fluctuation power in two opposing hemispheres is also found in the WMAP1 and COBE results (Eriksen et al. 2004b; Hansen et al. 2004). After the release of more WMAP results, similar large-scale anomalies are still detected in the WMAP3 data (Abramo et al. 2006; Jaffe et al. 2006; Copi et al. 2007; Land & Magueijo 2007; Eriksen et al. 2007; Park et al. 2007; Vielva et al. 2007; Samal et al. 2008) and WMAP5 data (Bernui & Hipolito-Ricaldi 2008) as well.

These apparent anomalies, if found to be cosmological origin, will pose a big challenge to the standard model of cosmology. Therefore, inspecting the effects of WMAP observation on released data at large angular scales more carefully is worth doing. We show in §2 that there exists in WMAP data a remarkable similarity between the large-scale non-Gaussian pattern of map temperatures and the distribution feature of observation numbers. Motivated from such a similarity, in this work we further check the

WMAP data for the correlation between pixel temperature t and observation number N . A systematic effect of imbalance differential observation and significant t - N correlation in magnitude, distribution non-Gaussianity and north-south asymmetry are detected and shown in §3. We give a brief discussion on the observation effect in WMAP data in §5.

2 LARGE-SCALE NON-GAUSSIAN MODULATION

To address the large scale anomalies, such as asymmetry, alignment and low l power issues detected in WMAP data with different techniques, the WMAP team (Spergel et al. 2006) describe the observed temperature fluctuations, \hat{t} , as a Gaussian and isotropic random field, \mathbf{t} , modulated by a function $f(\mathbf{n})$

$$\hat{t}(\mathbf{n}) = t(\mathbf{n})[1 + f(\mathbf{n})]$$

where $f(\mathbf{n})$ is an arbitrary modulation function. They expand $f(\mathbf{n})$ in spherical harmonics

$$f(\mathbf{n}) = \sum_{l=1}^{l_{max}} \sum_{l=-m}^m f_{lm} Y_{lm}(\mathbf{n})$$

and use maximum likelihood technique with a Markov Chain Monte Carlo solver to get the best fit values of f_{lm} with $l_{max} = 2$ for the WMAP3 V-band map. The top panel of Fig. 1 is obtained based on the best fit coefficients, showing in a unifying manner the large scale anomalies in WMAP temperature fluctuations which is the same feature that has been identified in a number of papers on non-Gaussianity.

The sky coverage of WMAP mission is inhomogeneous – the number of observations being greatest at the ecliptic poles and the

* E-mail: litp@tsinghua.edu.cn

† E-mail: liuhao@ihep.ac.cn

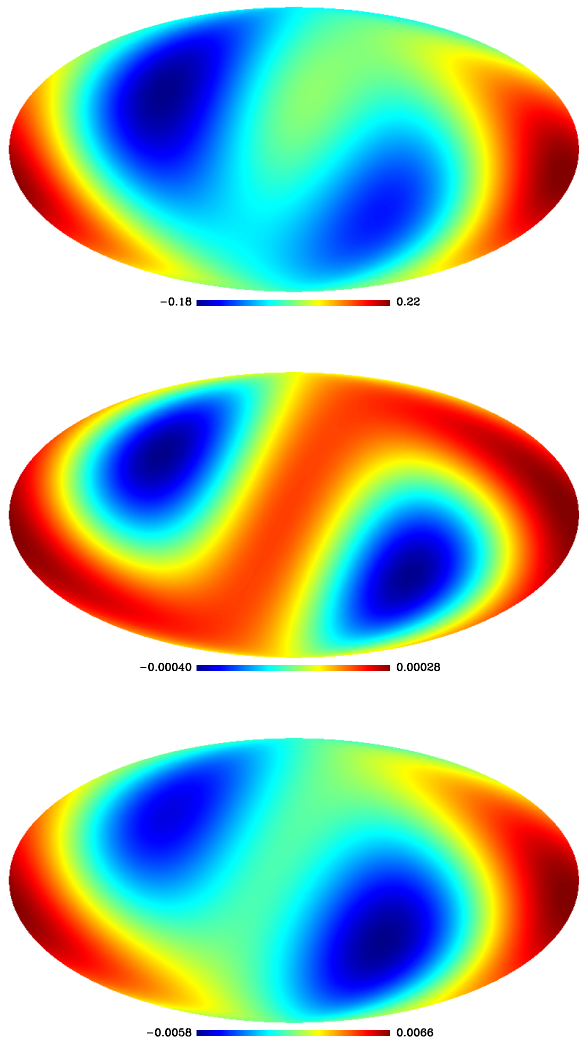


Figure 1. Large-scale non-Gaussian modulation features with $l_{max} = 2$ for the WMAP3 V-band data. *Top panel:* Best-fit large-scale modulation function $f(\hat{n})$ for temperature map. *Middle panel:* large-scale feature of $1/N$ map. *Bottom panel:* large-scale feature of $1/\sigma(N)$ map.

ecliptic plane being most sparsely observed (Hinshaw et al. 2007). To address the observation number distribution in the same way for the temperature distribution, we calculate the spherical harmonic coefficients f_{lm} with $l_{max} = 2$ for the map of $1/N$ with N being number of observations per sky pixel from the WMAP3 V-band data. The middle panel of Fig. 1 shows the map of $1/N$ reconstructed based on the coefficients f_{lm} . Comparing the two graphs at the top and middle of Fig. 1, we can see that the large-scale non-Gaussian modulation features of WMAP temperature map and scan pattern being similar for each other, showing considerable connection between pixel temperature t and observation number N .

We further show in the bottom panel the reconstructed result for the observation fluctuation map – the map of $1/\sigma(N)$ where the rms variation $\sigma(N) = \sqrt{\langle (N - \langle N \rangle)^2 \rangle}$ calculated within a region of $\sim 1^\circ$ side dimension for each sky pixel. From this map we notice, unexpectedly to some extent, that observation numbers in released WMAP data are also fluctuated. In comparing the three panels in Fig. 1, the modulation pattern for the observation fluctua-

tion map (the bottom panel) is more similar to the detected anomalies (the top panel), indicating that the fluctuation of observation numbers could produce additional uncertainty to the recovered temperature map.

3 TEMPERATURE-EXPOSURE COUPLING

3.1 t - N Correlation

The remarkable similarity between the large-scale non-Gaussian pattern of WMAP CMB temperatures and the distribution feature of observation numbers shown in the previous section prompts us to check the WMAP data for the correlation between pixel temperature t and observation number N . To inspect the t - N coupling, for a sky pixel i we calculate the correlation coefficient $C_{t-N}(i)$ by

$$C_{t-N}(i) = \frac{\sum_j (t_i(j) - \bar{t}_i)(N_i(j) - \bar{N}_i)}{\sqrt{\sum_j (t_i(j) - \bar{t}_i)^2 \sum_j (N_i(j) - \bar{N}_i)^2}}, \quad (1)$$

where the summations are taken over all WMAP pixels j (in the original resolution) within a spherical cap centered at the vertex i with an angular radius of 10° . We use Eq. 1 to produce a correlation map $C_{t-N}(i)$ from the WMAP5 Q-, V- and W-band data separately, where the vertexes i are defined with $r5$ resolution of HEALPix pixelization scheme (Gorski et al. 2005) in the sky sphere, if more than 20% of pixels of a cap are inside the Galactic mask KQ85 (Gold et al. 2008; Nolta et al. 2008), the cap is no longer used. From a correlation map, we calculate the average of absolute correlation coefficients $\langle |C_{t-N}| \rangle$ over the full sky, $\langle |C_{t-N}| \rangle_{south}$ over the South Galactic hemisphere, $\langle |C_{t-N}| \rangle_{north}$ over the north Galactic hemisphere, and the south-north asymmetry ratio $\langle |C_{t-N}| \rangle_{south} / \langle |C_{t-N}| \rangle_{north}$.

Now we use simulations to test the significance of the magnitude of $t - N$ correlation and its north-south asymmetry in WMAP data. The program synfast in HEALPix software package (available at <http://healpix.jpl.nasa.gov>) can create temperature maps computed as realizations of random Gaussian fields on a sphere characterized by the user provided spherical harmonic coefficients of an angular power spectrum. For each studied band, we produce 50,000 simulated temperature maps with the synfast program from the best fit Λ CDM model power spectrum (Nolta et al. 2008) with the beam function (Hill et al. 2008) and five-year like noise (Limon et al. 2003). We compute the average absolute value of $t - N$ correlation coefficient and its north-south asymmetry ratio for each simulated CMB map in the same way as for the WMAP5 data. Finally, we calculate the average and its standard deviation from 50,000 $\langle |C_{t-N}| \rangle$ and 50,000 $\langle |C_{t-N}| \rangle_{south} / \langle |C_{t-N}| \rangle_{north}$ respectively.

The obtained results are summarized in Table 1. From Table 1 we can estimate the significance of the average absolute magnitude of $t - N$ correlation being 4.68σ , 4.23σ and 4.78σ for Q-, V- and W-band respectively. Therefore, the $t - N$ coupling in WMAP5 data is much stronger than what expected from the Λ CDM model. In other words, the inhomogeneity of WMAP exposure may produce notable distortion in temperatures observed for the Λ CDM CMB. Especially, for each of the three bands, none of the 50,000 estimators $\langle |C_{t-N}| \rangle$ obtained from simulation exceeds the WMAP values in Table. 1. This is well consistent with the $\sim 4\sigma$ significance estimation for the three bands. From Table 1 we can also see a considerable north-south asymmetry existing in $t - N$ correlation with significance of 2.58σ , 2.18σ and 2.21σ for Q-, V- and W-band respectively.

Table 1. Average t - N correlation coefficients

		$\langle C_{t-N} \rangle$	$\frac{\langle C_{t-N} \rangle_{south}}{\langle C_{t-N} \rangle_{north}}$
Q-band	WMAP5	0.116	1.25
	Expectation	0.0837 ± 0.0069	1.010 ± 0.093
V-band	WMAP5	0.0977	1.20
	Expectation	0.0719 ± 0.0061	0.993 ± 0.095
W-band	WMAP5	0.0942	1.21
	Expectation	0.0660 ± 0.0059	0.995 ± 0.097

Furthermore, we test the Gaussianity of obtained WMAP t - N correlation distribution. Fig. 2 shows histograms of t - N correlation coefficients from WMAP5 Q-band data (solid line) and simulations (crosses and dotted line) for the Galactic north and south hemispheres separately. From Fig. 2 we see that, for both northern and southern hemispheres, the simulated t - N correlation coefficients are normally distributed, and the correlation coefficients measured from WMAP5 data visibly deviate from the normal distribution. The histogram of t - N correlation for the Galactic south hemisphere from WMAP5 Q-band data is much higher than the error bars at both tails, indicates that there are far more caps having strong t - N correlation than expected. On the contrary, the histogram for the north hemisphere is rather close to the simulation result. These results on non-Gaussianity and north-south asymmetry for t - N correlation distribution are consistent with that for t - N correlation magnitude.

The Kolmogorov-Smirnov test is also used to compare the measured (F) and simulated (F_0) cumulative distribution functions (CDFs). We find the maximum absolute differences (D_n) between the measured and simulated CDFs, $D_n = \max(|F - F_0|)$, is 0.105 for the north hemisphere and 0.185 for the south hemisphere, respectively. The threshold of D_n for null hypothesis $F = F_0$ at $\alpha = 0.01$ significance level and sample size, the used sky pixels $N_p \sim 4400$, is known to be $1.63/\sqrt{N_p} \approx 0.024$. The measured D_n are much higher than the threshold. Therefore, the null hypothesis $F = F_0$ has been rejected at $\alpha = 0.01$ or even higher significance level, indicating that the measured t - N correlation deviates significantly from simulation.

3.2 Effect of Imbalance Differential Observation

We find that the above results from the WMAP5 foreground-cleaned Q-band data with the KQ85 mask are almost the same with what obtained from the data without any mask; therefore, the detected t - N correlation can not be explained by the foreground effect. We will show that the instrumentation and observation effect can contribute to the observed t - N correlation and then distort observed temperature maps.

3.2.1 Differential observation

The COBE and WMAP missions measure temperature differences between sky points using differential radiometers consisting of plus-horn and minus-horn with a fixed separation angle θ_{beam} (Smoot et al. 1990; Bennett et al. 2003a). The beam separation angle of WMAP radiometers is $\theta_{beam} \sim 141^\circ$. Let denote t_i the temperature anisotropy at a sky pixel i . The raw data in a certain

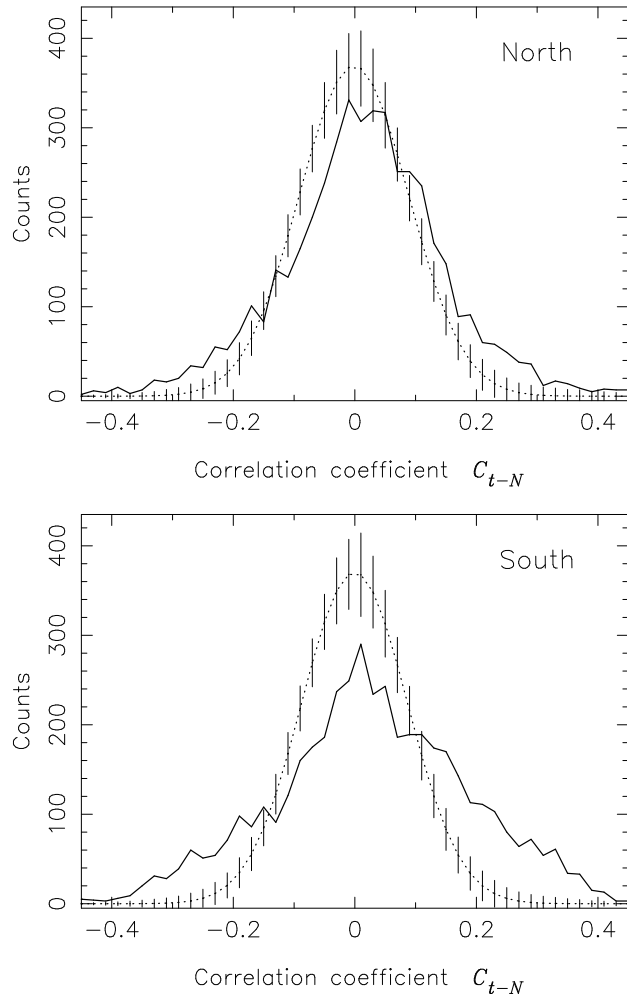


Figure 2. Histograms of t - N correlation coefficients. *Solid line:* from the WMAP5 Q-band data. *Dotted line:* expectation and 1σ error bar from 50000 simulations for the Λ CDM CMB. *Upper panel:* north hemisphere. *Lower panel:* south hemisphere.

band is a set of temperature differences \mathbf{d} between pixels in the sky. From N observations we have the following observation equations

$$\begin{aligned}
 t_{1+} - t_{1-} &= d_1 \\
 t_{2+} - t_{2-} &= d_2 \\
 &\dots\dots\dots \\
 t_{N+} - t_{N-} &= d_N,
 \end{aligned}$$

or in matrix notation

$$\mathbf{A}\mathbf{t} = \mathbf{d}. \quad (2)$$

Where the scan matrix $\mathbf{A} = (a(k, i))$, $k = 1, \dots, N$ and $i = 1, \dots, L$ with L being the total number of sky map pixels. The most of elements $a(k, i) = 0$ except for $a(k, i = k^+) = 1$ and $a(k, i = k^-) = -1$, where k^+ denotes the pixel observed by the plus-horn and k^- the pixel observed by the minus-horn at an observation k .

The normal equation of Eq. 2 is

$$\mathbf{M}\mathbf{t} = \mathbf{A}^T \mathbf{d} \quad (3)$$

with $\mathbf{M} = \mathbf{A}^T \mathbf{A}$.

The Eq. 3 can be expressed as

$$N_i^+ t_i - \sum_{k^+=i} t_{k^-} - \sum_{k^-=i} t_{k^+} + N_i^- t_i = \sum_{k^+=i} d_k - \sum_{k^-=i} d_k \quad (i = 1, 2, \dots, L).$$

Where $\sum_{k^+=i}$ means summing over N_i^+ observations while the pixel i is observed by the plus-horn and $\sum_{k^-=i}$ means summing over N_i^- observations while the pixel i is observed by the minus-horn, and the total number of observations for the pixel i is $N_i = N_i^+ + N_i^-$. From the above equations we can derive the following iterative formula

$$t_i^{(n+1)} = \frac{1}{N_i} \left(\sum_{k^+=i} (d_k + t_{k^-}^{(n)}) - \sum_{k^-=i} (d_k - t_{k^+}^{(n)}) \right) \quad (i = 1, 2, \dots, L). \quad (4)$$

With Eq. 4 when the number n of iteration is large enough, we get the final solution $\hat{t}_i = t_i^{(n)}$ for each pixel i . The Eq. 4 and the approximate iterative formula used by the WMAP team (Hinshaw et al. 2003), both have good performance for the differential data of a noiseless instrument.

3.2.2 Temperature distortion by instrument and observation imbalances

The differential data of WMAP contain errors caused by the instrument imbalance: the output of a WMAP radiometer from the plus-horn and mines-horn is not a purely differential response to sky signals (Jarosik et al. 2003; Jarosik et al. 2007). Instead of the ideal case $d_k = t_{k^+} - t_{k^-}$, a real observed differential data is

$$d_k = t_{k^+} - t_{k^-} + \delta_k, \quad (5)$$

where the difference distortion

$$\delta_k = x_{im}(t_{k^+} + t_{k^-}) \quad (6)$$

with the transmission imbalance factor x_{im} being valued between about 0.001 and 0.02 for different bands (Jarosik et al. 2007).

To roughly estimate the magnitude of the transmission imbalance effect on recovered temperatures, we use the first approximation derived from Eq. 4 with the initials $t_k^{(0)} = 0$

$$t_i^{(1)} = \frac{1}{N_i} \left(\sum_{k^+=i} d_k - \sum_{k^-=i} d_k \right). \quad (7)$$

Substituting Eq. 5 into Eq. 7 we get

$$t_i^{(1)} = \frac{1}{N_i} \left\{ \sum_{j=1}^{N_i^+} [t_i - t_j + \delta_j] - \sum_{j=N_i^++1}^{N_i} [t_j - t_i + \delta_j] \right\}, \quad (8)$$

where $j \in R_i$, R_i is the scan-ring with angular radius 141° to the pixel i . For N_i^+ observations $j = 1, \dots, N_i^+$, the plus-horn points

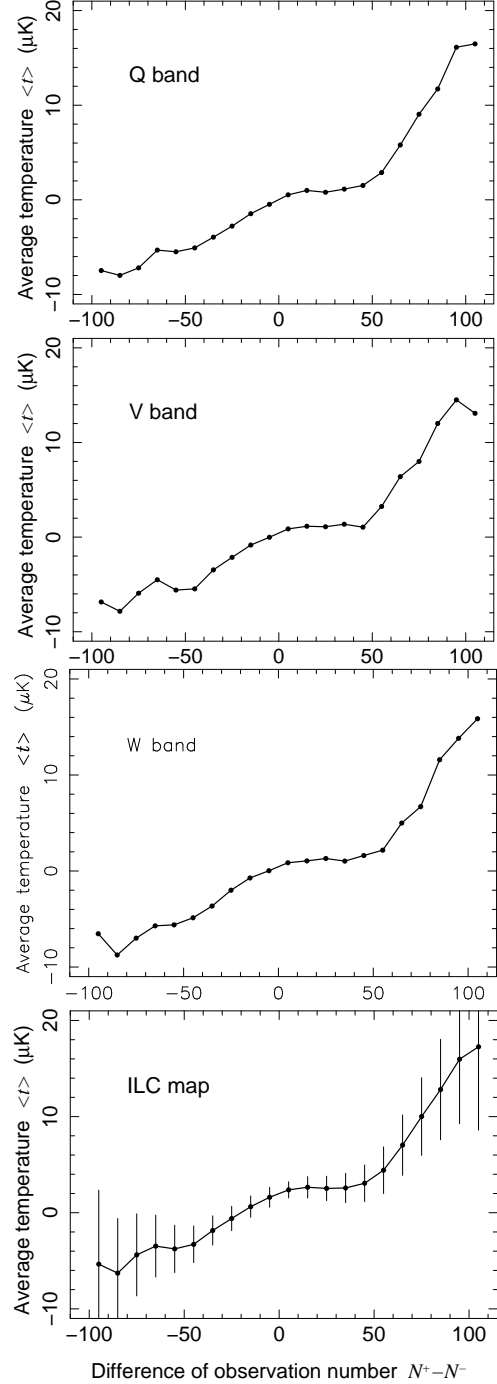


Figure 3. Average temperature vs. observation number difference $N^+ - N^-$ from WMAP5 data for Q-band, V-band, W-band and ILC maps. Error bars are only marked on the graph for ILC map, which are similar for other graphs.

to the pixel i and the mines-horn scans along the ring R_i ; and for N_i^- observations $j = N_i^+ + 1, \dots, N_i$, the mines-horn points to the pixel i and the plus-horn scans along the ring R_i . From Eq. 8 we can estimate the temperature distortion

$$t_i^{(1)} - t_i \simeq \frac{N_i^+ - N_i^-}{N_i} \bar{\delta}_R - \bar{t}_R, \quad (9)$$

where $\bar{t}_R = \sum_{j=1}^{N_i} t_j / N_i$, $\bar{\delta}_R = \sum_{j=1}^{N_i} \delta_j / N_i$ and $j \in R_i$.

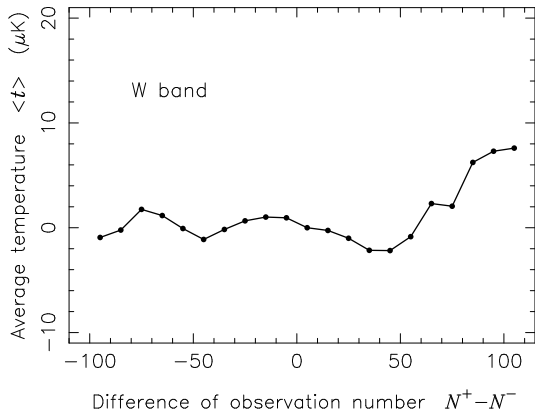


Figure 4. Average temperature vs. observation number difference $N^+ - N^-$ from WMAP5 W-band map after differential imbalance compensation with a compensate factor $\delta = 50 \mu\text{K}$.

From Eq. 9 we can see that a hot source contained on the scanning R_i will let the ring average temperature $\bar{t}_R \gg 0$ and the recovered temperature $t_i^{(1)} \ll 0$, in other words, a hot foreground source might systematically make the recovered temperatures on its scanning lower. We have indeed found such systematic distortion in released WMAP5 maps: scan-rings of hot sources are significantly cooled and strongest anti-correlations between pixel temperature and temperature of scan-ring with different separation angle θ appear at $\theta \sim 141^\circ$ (Liu & Li 2009).

Eq. 9 indicates that there might exist another kind of systematic distortion in recovered temperatures caused by transmission imbalance of radiometers through observation imbalance $N_i^+ \neq N_i^-$. Eq. 6 shows that the difference distortion δ_k of an observation k depends on the measured temperatures $t_{k+} + t_{k-}$. Although the transmission imbalance factor x_{im} is rather small, but the difference distortion δ_k can be considerable if any one of the measured temperatures is high enough. From Eq. 9 we see that for balance observations – the observation numbers of two horns $N_i^+ = N_i^-$, the difference distortion can not affect the recovered temperature. If the scan-ring R_i of pixel i contains hot sources and the observations are imbalance $N_i^+ \neq N_i^-$, the recovered temperature might be distorted. To check this effect, we arrange the temperatures t_i of all pixels i out of the foreground mask KQ75 from a released WMAP5 map in order of the observation number difference $\Delta N_i = N_i^+ - N_i^-$ from the WMAP5 TOD data. Fig. 3 shows the dependence of temperature averaged over a difference interval of 10 vs. difference ΔN between observation numbers by plus-horn and mines-horn. For Q-, V-, W-band and ILC maps, temperature distortions systematically changing along with ΔN as expected from above discussion on Eq. 9 are evidently exhibited in Fig. 3.

To roughly estimate the average magnitude of difference distortion, we try to correct the error by introducing a constant compensate factor δ for the WMAP5 differential data d_k to generate

$$d_k^* = d_k - \delta \quad (10)$$

and reconstruct a new temperature map from the correlated TOD data \mathbf{d}^* . Fig. 4 shows the $N^+ - N^-$ dependence from the new WMAP5 W-band map with $\delta = 50 \mu\text{K}$, where the observation imbalance effect is much mitigated. Fig. 3 and Fig. 4 show that temperature distortions caused by the transmission imbalance of radiometers are remarkable and scan-rings for pixels with strong

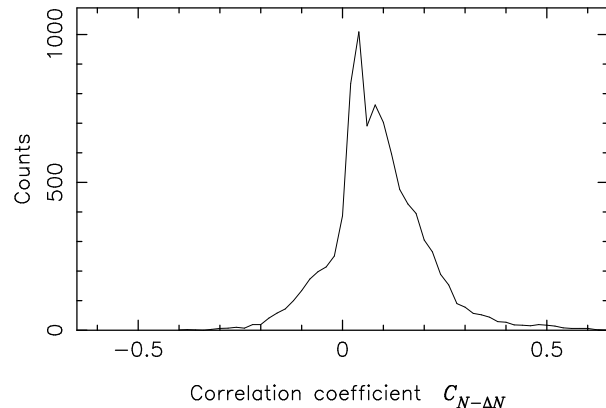


Figure 5. Histogram of ΔN - N correlation coefficients.

imbalance observations ($\Delta N > 50$) may generally contain hottest sources.

3.2.3 N - ΔN correlation

The dependence of average temperature $\langle t \rangle$ vs. observation number difference ΔN shown in Fig. 3 indicates that the input transmission imbalance of WMAP differential radiometers and unequal horn coverage ($\Delta N \neq 0$) may generate the t - N correlation observed in released WMAP maps, if a considerable N - ΔN correlation exists. To check it, we calculate correlation coefficients $C_{N-\Delta N}(i)$ from WMAP5 W1-band data with the same procedure we use to calculate $C_{t-N}(i)$ in §3.1: the correlation calculation summations are taken over all WMAP pixels j within a spherical cap centered at the vertex i with an angular radius of 10° , the vertexes i are defined with $r5$ resolution of HEALPix pixelization scheme in the sky sphere, if more than 20% of pixels of a cap are inside the Galactic mask KQ85 the cap is no longer used. Fig. 5 shows the histogram of correlation coefficients $C_{N-\Delta N}(i)$. From Fig. 5 we can see that strong correlation between the observation number N_i and difference $\Delta N_i = N_i^+ - N_i^-$ of a sky pixel i exists in observations used for making WMAP temperature maps. For most pixels i , the observation number N_i is positively correlated with the observation imbalance ΔN_i , then the temperature distortion by instrument and observation imbalances demonstrated in this section should contribute to the detected $t - N$ correlation presented in §3.1 through the N - ΔN correlation.

4 DISCUSSION

Unexplained large scale anomalies, e.g. the orientation of large-scale patterns in respect to the ecliptic frame, the north-south asymmetry of temperature fluctuation power etc, have detected in WMAP data. Their origin has long puzzled scientists. Several radical explanations with an anisotropic cosmology have already been proposed. However, it is, in particular, hard to imagine that there exists a special direction related to the ecliptic or Galactic plane in the early universe. In this work, we show that the large-scale features of the WMAP observation number map and observation number fluctuation distribution are very similar to the large-scale non-Gaussian modulation feature in released WMAP temperature map (§2), and find that significant correlation between pixel temperature and observation number exists in WMAP data (§3.1), such

correlation can be produced by the systematic effect of WMAP instrument and observation imbalances on temperature maps (§3.2). The detected observation number correlation should contribute, at least partly, to the apparent similarity between the large-scale features of the WMAP observation exposure and temperature maps, and hopefully provide a natural way to explain some large-scale anomalies in released WMAP temperature maps.

Inhomogeneity of observation numbers used in WMAP map-making is emerged at different sky scales, which should generate systematic errors in WMAP temperature maps in a wide range of angular scale through the significant t - N correlation revealed in this work. To limit systematic artifacts, a large amount works have been performed by the WMAP team. Due to the differential nature of WMAP observations, it is a difficult task. As an example, though the effect of input transmission imbalance from radiometer nonidealities has been noticed, calibrated and modified by the WMAP team (Jarosik et al. 2003; Jarosik et al. 2007), we still find remarkably systematic dependence of temperature vs. observation number difference between the two horns residual in released WMAP maps. As shown in §3.22, hotspots in the sky can distort recovered temperatures of pixels on large part of the sky with a complicated way. It has to be pointed out that using Eq. 10 with a constant compensation factor to correct the effect of horn imbalance is just to roughly estimate the average magnitude of differential imbalance distortion. What shown in Fig. 4 is only on the meaning of the average. More works have to be done to find a proper approach to modify the effect of imbalance differential observation to recover a corrected temperature map.

The real accuracy of cosmology parameters is the most important issue for high precision cosmology. Systematical temperature errors and structured noise fluctuations existed in CMB maps will certainly distort the angular power spectrum and the best-fit cosmology parameters as well. It is obviously needed to further study the errors in WMAP temperature and noise fluctuation maps caused by the observation inhomogeneity and imbalance. The systematic distortions detected by us in released WMAP maps come from the WMAP's differential nature. The next CMB mission Planck is designed to measure the CMB anisotropy with completely different mode and expected to be unaffected by such kind of distortions.

ACKNOWLEDGMENTS

The referees are thanked for their helpful comments and suggestions and Prof. S.N. Zhang for suggestion on presentation of detected non-Gaussianity of t - N correlation. This work is supported by the National Natural Science Foundation of China (Grant No. 10533020), the National Basic Research Program of China (Grant No. 2009CB-824800), and the Directional Research Project of the Chinese Academy of Sciences (Grant No. KJCX2-YW-T03). The data analyzed in this work are obtained through the HEASARC online service provided by the NASA/GSFC.

REFERENCES

- Abramo L.R., Bernui A., Ferreira I.S., Villela T. & Wuensche C.A., 2006, *Phys. Rev. D*, 74, 063560
 Bennett, C.L. et al., 2003a, *ApJ*, 583, 1
 Bennett, C.L. et al., 2003b, *ApJS*, 148, 1
 Bernui, A. & Hipolito-Ricaldi, W.S., 2008, *MNRAS*, 389, 1453
 Copi, C.J., Huterer, D., Schwarz, D.J. & Starkman, G.D., 2006, *MNRAS*, 367, 79
 Copi, C.J., Huterer, D., Schwarz, D.J. & Starkman, G.D., 2007, *Phys. Rev. D*, 75, 023507
 Cruz M., Martinez-Gonzalez E., Vielva P. & Cayon L., 2005, *MNRAS*, 356, 29
 Cruz M., Tucci M., Martinez-Gonzalez E. & Vielva P., 2006, *MNRAS*, 369, 57
 Cruz M., Cayon L., Martinez-Gonzalez E. & Vielva P., 2007a, *ApJ*, 655, 11
 Cruz, M., Turok, N., Vielva, P., Martinez-Gonzalez E. & Hobson M., *Science*, 2007b, 318, 1612
 de Oliveira-Costa, A., Tegmark, M., Zaldarriaga, & Hamilton A., 2004, *Phys. Rev. D*, 69, 063516
 Eriksen H.K., Hansen, F.K., Banday, A.J., Grski, K.M. & Lilje, P.B., 2004a, *ApJ*, 605, 14
 Eriksen H.K., Banday A.J., Gorski K.M. & Lilje, P.B., 2004b, *ApJ*, 612, 633
 Eriksen H.K., Banday, A.J., Grski, K.M. Hansen, F.K. & Lilje, P.B., 2007, *ApJ*, 660, L81
 Gold B. et al., 2008, arXiv:0803.0715
 Gorski, K. M., Hivon, E., Banday, A. J., Wandelt, B. D., Hansen, F. K., Reinecke, M., Bartelmann, M., 2005, *ApJ*, 622, 759
 Hansen F.K., Banday A.J. & Gorski K.M., 2004, *MNRAS*, 354, 641
 Hill, R.S., et al. 2008, arXiv:0803.0570
 Hinshaw, G. et al., 2003, *ApJS*, 148, 63
 Hinshaw, G. et al., 2007, *ApJS*, 170, 288
 Jaffe T.R., Banday A.J., Eriksen H.K., Gorski K.M. & Hansen F.K., 2005, *ApJ*, 629, L1
 Jaffe T.R., Banday A.J., Eriksen H.K., Gorski K.M. & Hansen F.K., 2006, *A&A*, 460, 393
 Jarosik, N. et al. 2003, *ApJS*, 148, 29
 Jarosik, N. et al. 2007, *ApJS*, 170, 263
 Land K. & Magueijo J., 2007, *MNRAS*, 378, 153
 Limon, M. et al., 2003, *Wilkinson Microwave Anisotropy Probe (WMAP) : Explanatory Supplement*, Greenbelt, MD: NASA/GSFC; Available in electronic form at <http://lambda.gsfc.nasa.gov/>
 Liu, H. & Li, T.P., 2009, *Sci China G-Phy Mech Astron*, in press; arXiv:0809.4160
 Nolta, M.R. et al., 2008, arXiv:0803.0593
 Park C.G., Park C. & Gott J.R., 2007, *ApJ*, 660, 959
 Samal, P.K., Saha, R., Jian, P. & Ralston, J.P., 2008, *MNRAS*, 385, 1718
 Schwarz, D.J., Starkman, G.D., Huterer, D. & Copi, C.J., 2004, *Phys. Rev. Lett.*, 93, 221301
 Smoot, G. et al. 1990, *ApJ*, 360, 685
 Spergel D. N. et al., 2006, arXiv:astro-ph/0603449v1
 Starkman, G.D. & Schwarz, D.J., 2005, *Sci. Am.*, 293(2), 48
 Vielva P., Wiaux Y., Martinez-Gonzalez E. & Vanderghenst P., 2007, *MNRAS*, 381, 932